INTERNATIONAL JOURNAL OF PRECISION ENGINEERING AND MANUFACTURING Vol. 15, No. 6, pp. 1035-1040 JUNE 2014 / 1035
DOI: 10.1007/s12541-014-0433-7

Structural Analysis on the Superficial Grooving Stainless-Steel Thin-Plate Rupture Discs

Jae Young Jeong[1], Wonseok Jo[1], Heungseob Kim[1], Seok Heum Baek[2], and Seong Beom Lee[1,#]

1 Department of Mechanical and Automotive Engineering, High Safety Vehicle Core Technology Research Center, Inje University, 607 Obangdong, Gimhae, Gyeongnam, South Korea
2 EN3S Team, DNDE Engineering, Ace Hightech21, Centumjungang-ro, Haeundae-gu, Busan, South Korea
Corresponding Author / E-mail: mechlsb@inje.ac.kr, TEL: +82-55-320-3667, FAX: +82-55-324-1723

KEYWORDS: Burst pressure prediction, Finite Element Analysis, Grooving process, Rupture disc

A rupture disc is a non-reclosing pressure-relief device actuated by inlet static pressure and designed to function by bursting a pressure-containing disc. It separates fluid from a safety relief valve, and thereby prevents leakage through the valve. Rupture discs are made from stainless steel, have a concave shape, and are designed to open at a predetermined pressure. They are used in safety-critical pressure-relief devices, and provide a leak-tight seal. In this paper, we describe a structural analysis and calculate the burst pressure of superficially grooved stainless-steel plate rupture discs. In general, rupture discs are designed based on a failure analysis of the material. We therefore conducted tensile tests on stainless-steel plate specimens to obtain their material properties, and then examined the relationship between the burst pressure and the thickness of the rupture disc using finite element analyses. Based on these results, we investigated the effects of groove depth and rupture disc thickness on burst pressure.

Manuscript received: April 15, 2013 / Revised: May 13, 2014 / Accepted: May 14, 2014

1. Introduction

A rupture disc (or bursting disc) is a non-reclosing pressure-relief device that provides a leak-tight seal. If the internal pressure of a vessel exceeds a predetermined level, the rupture disc bursts, providing rapid, unobstructed relief of the overpressure, preventing damage to equipment and potentially hazardous situations. Cross-scored rupture discs operate in response to reverse-acting compression loads, and the scored pattern on the surface facilitates opening without fragmentation. It is important to manufacture cross-scored rupture discs to fail at a predetermined pressure in safety-critical industrial applications.[1-4]

Lee et al.[5] recently reported an analysis of cross-scored rupture discs employing a finite element method and elastic material models. In the present work, we conducted a structural analysis for superficially grooved stainless-steel thin-plate discs by applying a specified burst pressure. We then defined their manufacturing design range based on the results of finite element analyses.

2. Material Property Tests

Fig. 1 shows a rectangular tensile test specimen as specified in Ref. 6. Figs. 2(a)~(d) show tensile test specimens of SUS 316L stainless-steel plate, and Fig. 2(e) shows the tensile test apparatus (Instron 8810) based on Ref. 7.

Fig. 3(a) shows force-displacement curves of SUS 316L stainless-steel plate of various thicknesses, taken from Ref. 5. The stress-strain curve obtained from the force-displacement data is shown in Fig. 3(b). Table 1 summarizes the material data for SUS 316L stainless steel.

3. Finite Element Analysis

3.1 Material properties

Fig. 4 shows the material properties used in the finite element model for the superficially grooved stainless-steel thin-plate rupture discs. Bilinear isotropic hardening (BISO) uses the von Mises yield criteria coupled with an isotropic work hardening assumption. The Young's modulus and yield stress at 260°C were taken into account as per Ref. 8; these values are listed in Table 2, where RF = reduction factor.

3.2 Finite element model

The finite element model for the superficially grooved stainless-steel thin-plate rupture discs was based on SOLID185 elements, and

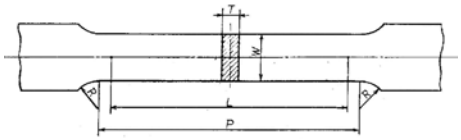

Fig. 1 Standard tensile test specimen: KS B 0801 No. 5 (W=25 mm, L=50 mm, P=60 mm, R=15 mm, and T=t=0.3, 0.4, 0.5, and 0.6 mm)

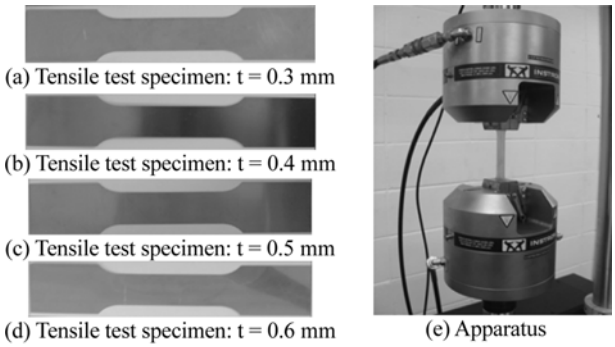

Fig. 2 Tensile test specimens and apparatus

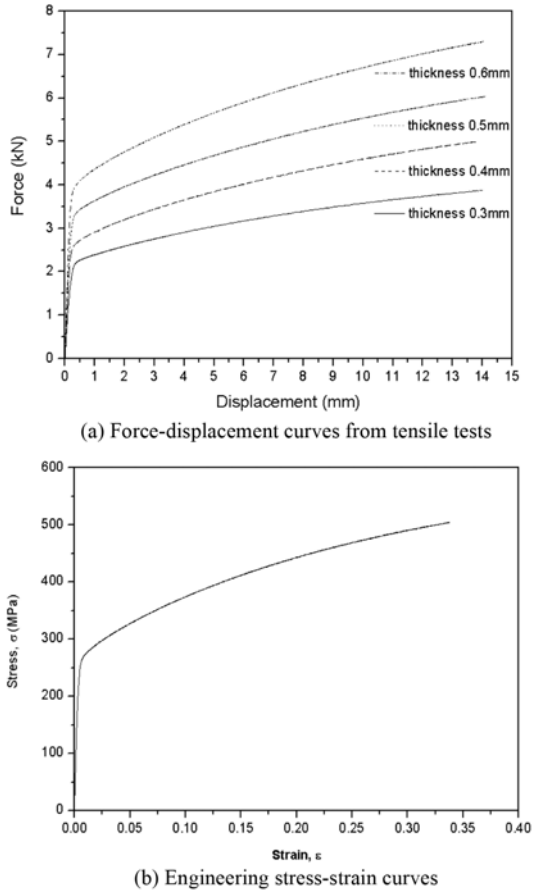

Fig. 3 Material data for SUS 316L stainless steel from Ref. 5. (a) In-plane tensile force-displacement curves, (b) Resulting stress-strain curve

consisted of a cyclically symmetric quarter-sector model. The various design parameters used for the finite element modeling are illustrated in Fig. 5 and listed in Table 3. The finite element models are shown in

Table 1 Material data for SUS316L stainless steel

Temp. (°C)	Young's modulus (MPa)	Tangent modulus (MPa)	Yield stress (MPa)	Tensile stress (MPa)	Poisson's ratio (-)
20	78975	906.7	260.425	520.475	0.29

Table 2 Young's modulus and yield stress for SUS316L stainless steel

Temp. (°C)	Young's modulus (MPa)	Yield stress (MPa)
260	70366 {=78975(20°C)×0.891(RF)}	243.237 {=260.425(20°C)×0.934 (RF)}

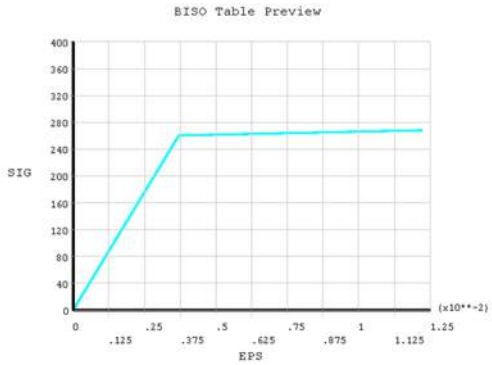

Fig. 4 Material properties (BISO) used in the finite element model of the superficially grooved stainless-steel thin-plate rupture discs

Table 3 Design parameters (mm) used for the finite element model

t	gt	gw	r	h	w1	w2
0.3	0.06	38.6	52.0	7.0	0.8	8.0
	0.09					
	0.12					
	0.14					
0.4	0.09					
	0.12					
	0.17					
	0.23					
0.5	0.13					
	0.18					
	0.23					
	0.30					
0.6	0.15					
	0.20					
	0.25					
	0.30					

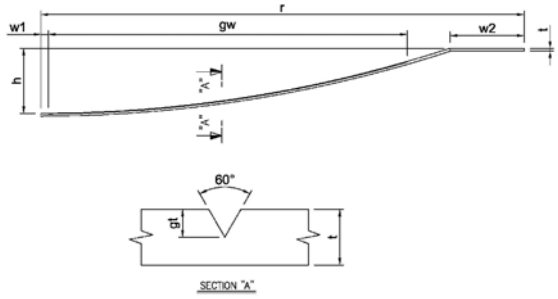

Fig. 5 Description of the design parameters

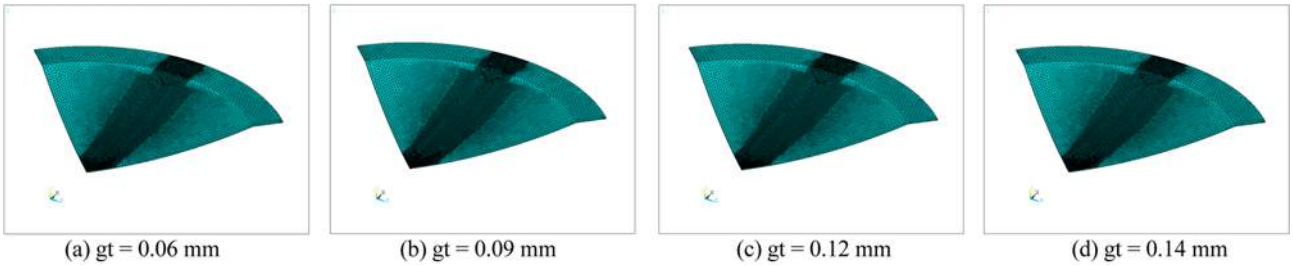

Fig. 6 Finite element model of the rupture disc: t=0.3 mm

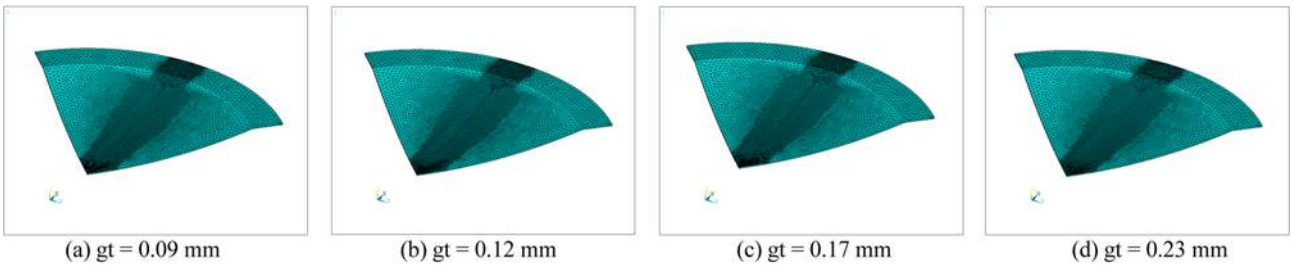

Fig. 7 Finite element model of the rupture disc: t=0.4 mm

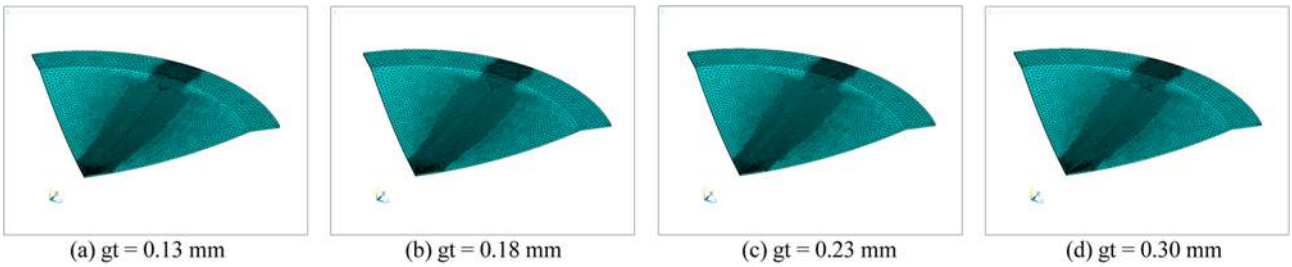

Fig. 8 Finite element model of the rupture disc: t=0.5 mm

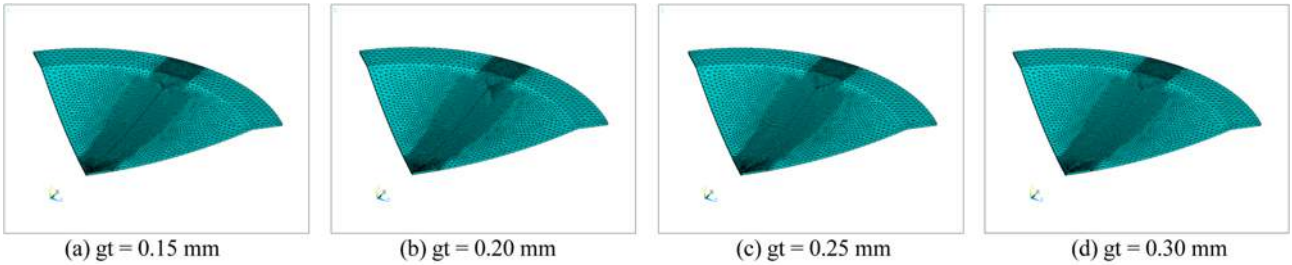

Fig. 9 Finite element model of the rupture disc: t=0.6 mm

Figs. 6~9. SOLID185 elements were defined by eight nodes with three degrees of freedom at each node (translation in the nodal x, y, and z directions). These elements have plasticity, hyperelasticity, stress stiffening, creep, large deflection, and large strain capabilities.[9]

3.3 Boundary conditions

The boundary conditions for the finite element analysis were set to avoid rigid-body motion and to take advantage of the cyclic symmetry of the quarter-sector model shown in Fig. 10. The displacement of nodes on the two side faces of the cyclic symmetric quarter-sector model was zero, using cyclic coupling in the nodal coordinate system (cylindrical, C.S = 5). The nodes at the top and bottom of dimension parameter w2 (see Fig. 5), which were in contact with rupture disc holder, were constrained by zero displacement in the circumferential and vertical directions of the local cylindrical coordinate system (cylindrical, L.C.S = 1).

The burst pressure (Pb = 0.689 MPa) specified in Ref. 5 was applied to the convex side of the finite element model, as shown in Fig. 11.

3.4 Analysis results

An elastic-plastic stress analysis was performed using the finite element models of the superficially grooved stainless-steel thin-plate

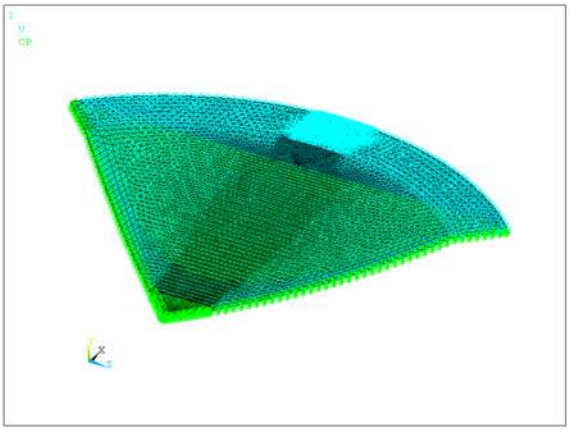

Fig. 10 Boundary conditions for the finite element model of the rupture disc

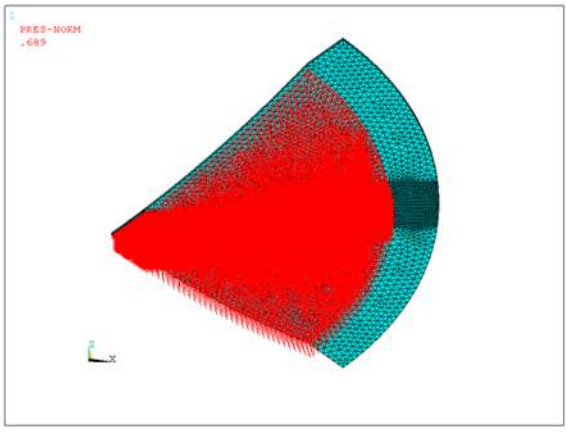

Fig. 11 Specified burst pressure (Pb = 0.689 MPa) for the finite element model of the rupture disc

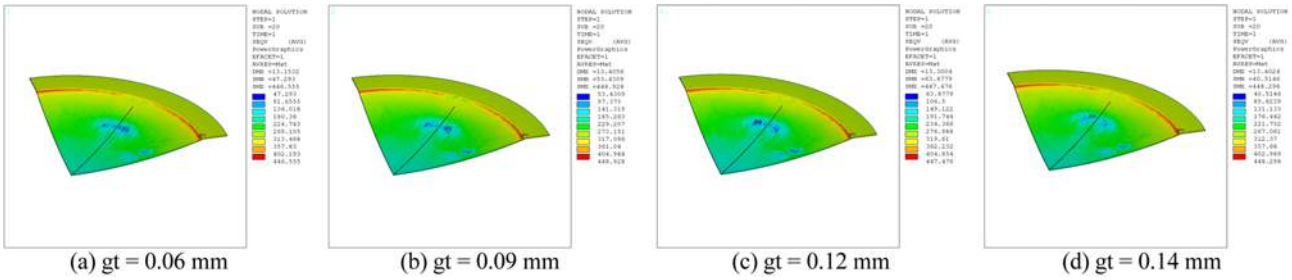

Fig. 12 Finite element model results for the rupture disc: t=0.3 mm

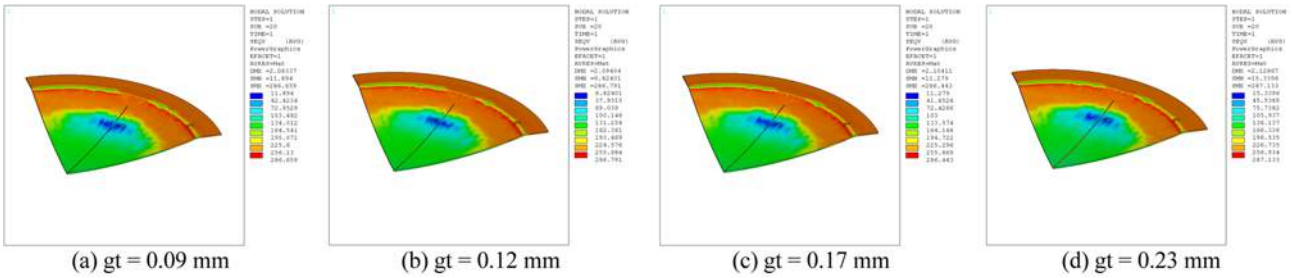

Fig. 13 Finite element model results for the rupture disc: t=0.4 mm

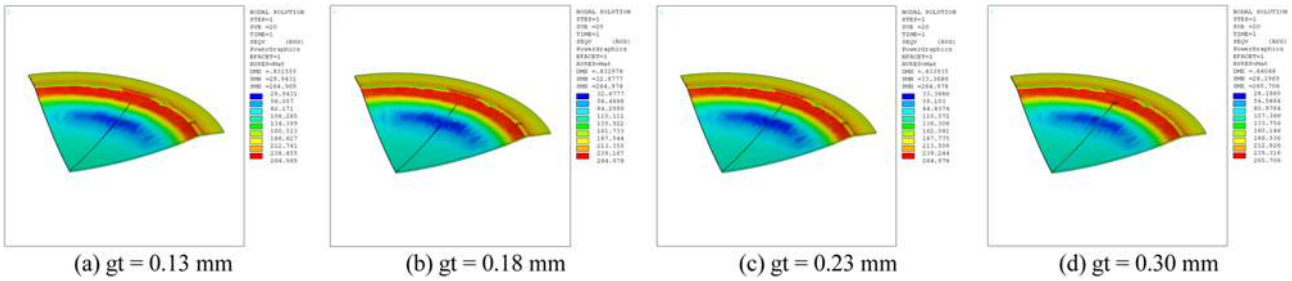

Fig. 14 Finite element model results for the rupture disc: t=0.5 mm

rupture discs. An elastic-plastic stress analysis provides a more accurate assessment of the plastic collapse of a component relative to the criteria because the actual structural behavior is more closely approximated. The stress redistribution that occurs as a result of inelastic deformation (plasticity) and the deformation characteristics of the component are considered directly in the analysis. The plastic collapse load can be obtained using a finite element method by incorporating an elastic-plastic material model to obtain a solution. The effects of non-linear

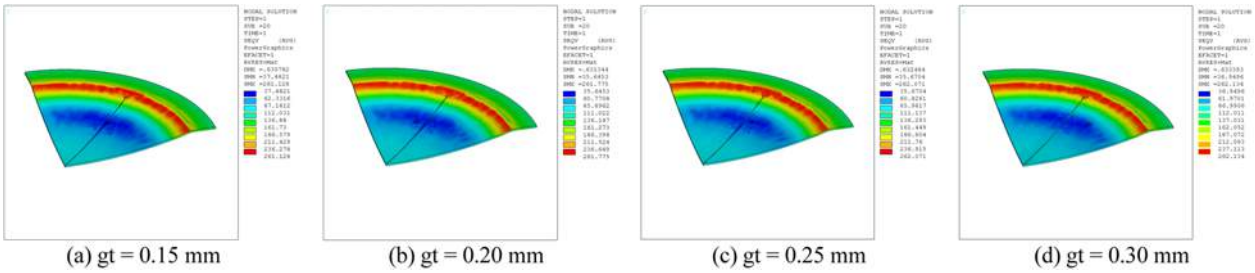

Fig. 15 Finite element model results for the rupture disc: t=0.6 mm

geometries are also considered in this analysis. The plastic collapse load is the load that causes the overall structural instability.[10]

Figures 12~15 show the analysis results for the superficially grooved stainless-steel thin-plate rupture discs.

3.5 Evaluation method

The total stress distribution of the specimens was obtained from the finite element analyses (see Figs. 12~15). Therefore, to calculate the local primary membrane equivalent stress (P_L), the total stress distribution was linearized on a stress-component basis and used to determine the equivalent stresses. The local primary membrane equivalent stress (P_L) develops on cross-sections through the thickness of the specimens. These sections are known as stress classification planes (SCPs). In a planar geometry, a stress classification line (SCL) is obtained by reducing two opposite sides of an SCP to an infinitesimal length. SCPs are flat planes that cut through a section of a component, and SCLs are straight lines that cut through a section of the specimen.

Superficially grooved stainless-steel thin-plate rupture discs contain structural discontinuity regions with abrupt changes in geometry. These regions are typically located at the regions of the highest stress. For the evaluation of failure modes of plastic collapse, the SCL is located at gross structural discontinuities. And, for the evaluation of local failure, SCL is located at local structural discontinuity, so we evaluated local failures; the SCL was located as shown in Fig. 16.

The explosion condition of superficially grooved stainless-steel thin-plate rupture discs at the specified burst pressure (Pb = 0.689 MPa) is such that the local primary membrane equivalent stress (P_L) located at local structural discontinuity exceeds the maximum allowable stress ($2/3 \times Sy$): [9,11]

Local primary membrane equivalent stress (P_L) > $1.5 \times 2/3 \times Sy$

where $2/3 \times Sy$ is the maximum allowable stress at 260°C, so

$Sy = 260.425$ (20°C) $\times 0.934$ (RF) $= 243.237$ MPa

$2/3 \times Sy = 2/3 \times 243.24$ MPa $= 162.16$ MPa

$1.5 \times 2/3 \times Sy = 1.5 \times 162.2$ MPa $= 243.2$ MPa

3.6 Evaluation of analysis results

Table 4 presents the evaluation of analysis results for the superficially grooved stainless-steel thin-plate rupture discs.

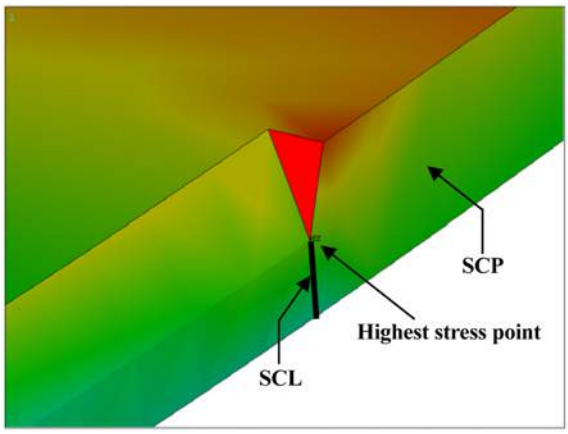

Fig. 16 Location of the SCL and SCP in the superficially grooved stainless-steel thin-plate rupture discs

Table 4 Evaluation of the analysis results

t	gt	P_L	1.52/3×Sy	Evaluation
0.3	0.06	233.8	243.2	No explosion
	0.09	258.2	243.2	Explosion
	0.12	268.9	243.2	Explosion
	0.14	276.9	243.2	Explosion
0.4	0.09	252.8	243.2	Explosion
	0.12	248.9	243.2	Explosion
	0.17	244.4	243.2	Explosion
	0.23	228.9	243.2	No explosion
0.5	0.13	212.6	243.2	No explosion
	0.18	211.1	243.2	No explosion
	0.23	194.0	243.2	No explosion
	0.30	174.3	243.2	No explosion
0.6	0.15	152.2	243.2	No explosion
	0.20	141.9	243.2	No explosion
	0.25	138.7	243.2	No explosion
	0.30	141.3	243.2	No explosion

4. Conclusions

In this study, material property tests for SUS 316L stainless steel were carried out and the experimental data were applied to a finite element model of superficially grooved stainless-steel thin-plate rupture discs with design parameters to define the manufacturing design range at specified explosion conditions by performing finite element analysis. From this study, the following results were obtained.

(1) From the evaluation result for thickness of the rupture disc, t = 0.3 mm with grooving thickness, gt = 0.06, 0.09, 0.12, 0.14 mm, explosion due to local failure is increasing in proportion to the grooving thickness. The minimum grooving thickness is gt = 0.0715

mm at a specified explosion conditions using linear interpolation method.

(2) From the evaluation result for thickness of the rupture disc, t = 0.4 mm with grooving thickness, gt = 0.09, 0.12, 0.17, 0.23 mm, explosion due to local failure is decreasing in proportion to the grooving thickness. The maximum grooving thickness is gt = 0.156 mm at a specified explosion conditions using linear interpolation method.

(3) From the evaluation result for thickness of the rupture disc, t = 0.5 mm with grooving thickness, gt = 0.13, 0.18, 0.23, 0.30 mm, explosion due to local failure is little correlation to the grooving thickness.

(4) From the evaluation result for thickness of the rupture disc, t = 0.6 mm with grooving thickness, gt = 0.15, 0.20, 0.25, 0.30 mm, explosion due to local failure is little correlation to the grooving thickness.

Therefore the superficially grooved stainless-steel thin-plate rupture discs with design parameters (t = 0.3 mm: gt = 0.09, 0.12, 0.14 mm and t = 0.4 mm: gt = 0.09, 0.12, 0.17 mm) is expected to burst at a specified explosion conditions (Pb = 0.689 MPa, Temperature = 260°C) as manufacturing design range.

We proposed a numerical analysis technique involving an evaluation method that can be used to certify the capacity of rupture discs, thereby avoiding hazardous experimental bursting tests (e.g., hydrostatic or pneumatic tests).

In future work, we plan to experimental bursting test for the superficially grooved stainless-steel thin-plate rupture discs with design parameters and compare with the analysis results.

ACKNOWLEDGEMENT

This work was supported by the 2013 Inje University research grant.

REFERENCES

1. Wu, D., Peddieson, J., Buchanan, G. R., and Rochelle, S. G., "Estimation of Disk Burst Pressures using Limit analysis Collapse Loads," Journal of Pressure Vessel Technology, Vol. 124, No. 4, pp. 493-494, 2002.
2. Xue, L., Widera, G. E. O., Sang, Z., "Parametric FEA Study of Burst Pressure of Cylindrical Shell Intersections," Journal of Pressure Vessel Technology-Transactions of The ASME, Vol. 132, No. 3, Paper No. 031203, 2010.
3. Kisioglu, Y., "Burst Pressure Determination of Vehicle Toroidal Oval Cross-Section LPG Fuel Tanks," Vol. 133, No. 3, Paper No. 031202, 2011.
4. Jones, D. P. and Holliday, J. E., "Elastic-Plastic Analysis of the PVRC Burst Disk Tests With Comparison to the ASME Code Primary Stress Limits," Journal of Pressure Vessel Technology, Vol. 122, No. 2, pp. 146-151, 2000.
5. Jeong, J. Y., Lee, J., Yeom, S., Choi, W., Kim, T. G., and et al., "A Studt on the Grooving Process of a Cross-scored Rupture Disc," Int. J. Precis. Eng. Manuf., Vol. 13, No. 2, pp. 219-227, 2012.
6. Korean Industrial Standards, "The Pieces for Tension Test for Metallic Materials," KS B 0801, 1981.
7. Korean Industrial Standards, "Method of Tensil Test for Metallic Materials," KS B 0802, 1998.
8. API Recommended Practice, "Recommended Practice for the Design of Offshore Facilities against Fire and Blast Loading," 2006.
9. ASME, "BPVC Section VIII-Rules for Construction of Pressure Vessels Division 1," 2010.
10. ANSYS Inc., "ANSYS 13.0 User's Manual," 2010.
11. ASME, "BPVC Section VIII-Rules for Construction of Pressure Vessels Division 2-Alternative Rules," 2010.